Human osteoblast response to uncemented knee implant surface structures and osteoclast formation in vitro

Puijk, R.; Zandieh-Doulabi, B.; Runderkamp, W.J.A.M.; Pijls, B.G.; Klein-Nulend, J.; Nolte, P.A.

Hard Tissues and Materials

JOURNAL OF biomaterials applications

Journal of Biomaterials Applications
2025, Vol. 40(5) 580–590

DOI: 10.1177/08853282251346324
journals.sagepub.com/home/jba
Sage

Human osteoblast response to uncemented knee implant surface structures and osteoclast formation in vitro

Raymond Puijk[1,2], Behrouz Zandieh-Doulabi[2], Wendy J.A.M. Runderkamp[2], Bart G. Pijls[3], Jenneke Klein-Nulend[2] and Peter. A. Nolte[1,2]

Abstract

Early bone ingrowth and minimal resorption ensure rigid fixation in uncemented total knee replacements. Trabecular titanium–aluminum–vanadium (Ti6Al4V) and hydroxyapatite (HA)-coated vacuum-plasma-sprayed (VPS) titanium with varying porosities and HA-coating thicknesses, have been developed to enhance fixation, though bone cellular response remains largely unknown. This study evaluated osteoblast responses to trabecular Ti6Al4V and three VPS titanium surfaces with 20%–40% or 30%–70% porosity and HA coatings of 60, 80, or 90 μm. Human primary osteoblasts were seeded and cultured for 29 days, to assess seeding efficiency, viability, metabolic activity, alkaline phosphatase activity, and the effect of osteoblast-released factors in conditioned medium during the last 4 days of culture on osteoclast formation. VPS-HA groups were first compared individually; when no differences were found, data were pooled for comparison with the trabecular group. Osteoblast seeding efficiency, viability, metabolic activity, and alkaline phosphatase activity were similar between VPS-HA surfaces. Moreover, osteoblast-conditioned medium did not affect osteoclast formation. Osteoblast seeding efficiency and viability were similar between the pooled VPS-HA and trabecular surface. Compared to the pooled VPS-HA, the trabecular surface increased osteoblast metabolic (1.5-2.7-fold) and alkaline phosphatase activity (6.5-15.2-fold). Osteoblast-conditioned medium reduced osteoclast formation (2.1-3.4-fold) on trabecular compared to the pooled VPS-HA surface. In conclusion, these findings show that VPS-HA surfaces with various porosities and HA-coating thicknesses similarly affect osteoblast and osteoclast responses, while trabecular surfaces enhance osteoblast responsiveness and inhibit osteoclast formation. These results might help to further improve early stability and reduce long-term loosening risk in uncemented knee replacements.

Keywords

Osteoblast, osteoclast, surface, total knee replacement, uncemented

Introduction

Total knee arthroplasty is one of the most commonly performed elective procedures worldwide, with approximately 1.5 million surgeries performed annually worldwide.[1] While cemented total knee replacements (TKR) are predominantly used, their long-term durability is a concern, particularly in younger, more active, and heavier patients who place greater mechanical stress on implants.[1] With total knee arthroplasty demand projected to grow 43%–68% by 2050, and aseptic loosening as the leading cause of failure, uncemented TKR relying on biological fixation is considered a promising solution.[1]

Innovations in uncemented TKA focus on surface modifications to enhance biocompatibility, osteoinduction,

[1]Department of Orthopaedics, Spaarne Gasthuis, Hoofddorp, The Netherlands
[2]Department of Oral Cell Biology, Academic Centre for Dentistry Amsterdam (ACTA), University of Amsterdam and Vrije Universiteit Amsterdam, Amsterdam Movement Sciences, Amsterdam, The Netherlands
[3]Department of Orthopaedics, Leiden University Medical Center (LUMC), Leiden, The Netherlands

Corresponding author:
Behrouz Zandieh-Doulabi, Department of Oral Cell Biology, Academic Centre for Dentistry Amsterdam (ACTA), University of Amsterdam and Vrije Universiteit Amsterdam, Amsterdam Movement Sciences, Gustav Maherlaan 3004, Amsterdam 1081LA, The Netherlands.
Email: bzandiehdoulabi@acta.nl

and osseointegration.[2] Modifying surface morphology (i.e., roughness, porosity, pore size, interconnectivity), with or without coatings such as hydroxyapatite (HA), strongly influence osteoblast adhesion, proliferation, and differentiation.[2–5] These advancements aim to enhance implant-bone fixation, reduce the risk of aseptic loosening, and improve implant longevity.

Radiostereometric analysis (RSA) is a precise imaging method used to measure implant migration in vivo.[6] RSA studies show that early migration within 2 years predicts late failure by aseptic loosening (5–15 years), supporting the theory that insufficient early bone ingrowth—due to fibrous membrane formation or osteoclast-induced bone resorption—is a key factor in implant loosening.[6,7] Despite its importance for net bone gain, the role of osteoblast-released factors in regulating osteoclast formation and bone resorption remains underexplored.[3,4,8] In uncemented TKA, relatively new surface technologies include highly porous trabecular surfaces and vacuum-plasma-sprayed (VPS) titanium (Ti), often combined with hydroxyapatite (HA) coating. These technologies are applied in pockets (i.e., impressed areas on the implant), with pocket depth determining the thickness of the applied surface modification. Pocket depth itself varies along a component based on the required cross-sectional implant thickness to ensure adequate mechanical strength.[9] Previous RSA studies suggest that trabecular surfaces stabilize faster than porous HA-coated surfaces, potentially improving initial fixation, but mid- to long-term data on aseptic loosening risks are lacking due to their relatively recent introduction in clinical use.[10,11]

The aim of this study was to evaluate the osteoblast response to trabecular titanium–aluminum–vanadium (Ti6Al4V) surfaces and hydroxyapatite (HA)-coated vacuum-plasma-sprayed (VPS) titanium (Ti) surfaces with varying pocket depths, porosity, and HA-coating thicknesses: 350 µm pocket depth with 20%–40% porosity and 60 µm HA (VPS350-HA), 400 µm pocket depth with 30%–70% porosity and 90 µm HA (VPS400-HA), and 1000 µm pocket depth with 30%–70% porosity and 80 µm HA (VPS1000-HA). Trabecular Ti surfaces were applied to Ti6Al4V alloy discs, while HA-coated VPS Ti surfaces were applied to cobalt–chromium–molybdenum (CoCrMo) alloy discs.

Both Ti6Al4V and CoCrMo alloys are commonly used in uncemented TKR in clinical practice, with different pocket depths applied based on implant location and mechanical requirements.[2,10] Human primary osteoblasts were seeded on the trabecular Ti6Al4V or HA-coated VPS Ti surfaces and cultured for up to 29 days to assess seeding efficiency, viability, metabolic activity, alkaline phosphatase activity, and the effect of osteoblast-released factors in conditioned medium (CM) harvested during the last 4 days of culture on osteoclast formation. Comparisons were first made between the individual VPS-HA groups and subsequently pooled to compare with the trabecular surface. Our findings indicated a differential response of osteoblasts to HA-coated VPS surfaces on Ti with various porosity compared to trabecular-Ti surface.

Materials and methods

This study complies with the Preferred Reporting Items for Laboratory studies in Endodontology (PRILE) guidelines, and includes the PRILE checklist (Table S-1).[12]

Scaffolds and surfaces

A total of 48 disc-shaped scaffolds (25 mm diameter, 3.5 mm height) were used, consisting of a base disc with distinct upper surfaces. Of these, 36 CoCrMo alloy discs featured a VPS of commercially pure Ti, coated with HA, and were divided into three groups: VPS350-HA (300 µm Ti-layer, 20%–40% porosity, 60 µm HA), VPS400-HA (400 µm Ti-layer, 30%–70% porosity, 90 µm HA), and VPS1000-HA (1000 µm Ti-layer, 30%–70% porosity, 80 µm HA). These VPS-HA modifications are based on the "MectaGrip" technology[13] of Medacta International (Castel San Pietro, Switzerland), which is used in the uncemented Global Medacta Knee TKR. The remaining 12 scaffolds consisted of Ti6Al4V alloy discs with a 1000 µm 3D-printed trabecular Ti6Al4V honeycomb structure, corresponding to Medacta Internationals "3D-Metal" technology[13] which is being considered for use in their uncemented TKR. All scaffolds were provided by Medacta International, and their characteristics are summarized in Table 1. All scaffolds were sterilized using gamma radiation followed by UV sterilization prior to use.

Cell culture and seeding onto the scaffolds

Commercially obtained primary osteoblasts (passage (2) isolated from the femoral heads of 3 healthy female donors (aged 64–85 years) were used (Catalogue CC-12720; PromoCell, Huissen, The Netherlands). Osteoblasts were grown and maintained in phenol red-free Dulbecco's Modified Eagle Medium (DMEM) supplemented with 5% human platelet lysate (Sanquin, Amsterdam, The Netherlands), 1% penicillin/streptomycin/fungizone (PSF; Sigma-Aldrich, Saint Louis, MO, USA), and 0.2% heparin (5000 IU/ml; LEO Pharma A/S, Ballerup, Denmark). They were maintained in a humidified incubator with 5% CO_2 in air at 37°C until they reached approximately 80% confluency, yielding a minimum of 5×10^6 cells per donor. At the time of, the mean passage number was 5 (range: 4–7). Cells were detached from culture flasks using 0.25% trypsin (Gibco, Invitrogen, Waltham, MA, USA), counted using a Muse Cell Analyzer (Merck, Burlington, MA, USA), and resuspended in culture medium with additives. Ten 100 µL drops of the cell suspension were carefully spread all over the scaffolds surface at 1.0×10^5 cells/cm^2 scaffold (VPS-Ti-HA of 5.0 cm^2; trabecular 25.0 cm^2) in 6-well culture

Table 1. Characterizations of the different scaffolds, including the ground disc and surface.

	Pooled VPS-HA			
Scaffold name	VPS350-HA	VPS400-HA	VPS1000-HA	Trabecular
Ground disc				
Alloy	CoCrMo	CoCrMo	CoCrMo	Ti6Al4V
Surface				
Material/alloy	Ti	Ti	Ti	Ti6Al4V
Thickness, μm	350	400	1000	1000
Porosity, %	20-40	30-70	30-70	65-80
Pore void space, μm	100-350	100-350	100-350	450-900
Interconnecting pores	No	No	No	Yes
Coating	HA	HA	HA	-
Coating thickness, μm	60	90	80	-

VPS vacuum plasma-spray; CoCrMo, cobalt–chromium–molybdenum; Ti6Al4V, titanium–aluminum–vanadium, Ti Titanium, HA Hydroxyapatite.

plates (Greiner, Bio-One, Alphen aan de Rijn, The Netherlands). Attachment was allowed for 30 min, and osteogenic medium was added to cell/scaffold constructs. The osteogenic culture medium was composed of phenol red-free DMEM, 2% human platelet lysate, 1% PSF, 1% ascorbic acid (50 μg/mL), β-glycerophosphate (10 nM), and 0.2% heparin (5000 IU/ml), and was refreshed twice a week. To obtain osteoblast-CM, the medium was changed to phenol red-free α-Minimum Essential Medium (α-MEM; Gibco, Life Technologies, Waltham, MA, USA), 10% fetal bovine serum (FBS; Gibco, Life Technologies), 1% PSF, 1% ascorbic acid, and 1% BGP at day 25, and collected at day 29. This osteoblast-CM was used in experiments to compare the effect of soluble factors produced by osteoblasts cultured on the different scaffold surfaces on osteoclast formation.

Osteoblast seeding efficiency

To determine the number of cells that attached to the different scaffolds, seeding efficiency and viability were assessed after 16–24 hours. All scaffolds were transferred to new 6-well plates, and the cells remaining in the original plates were counted after trypsinization using a Muse Cell Analyzer (Merck, Burlington, MA, USA). Seeding efficiency was calculated by taking the number of initially seeded cells, subtracting the cells that attached to the original plate, dividing by the total cells attached to the scaffold, and multiplying by 100 to obtain a percentage. Data were obtained from three donors (n = 3), with experiments in duplicate.

Attachment of osteoblasts

To assure that cells were attached to the different scaffolds after 4 days, a total of three scanning electron microscope (XL20, Fei Company, Eindhoven, The Netherlands) images were carried from three replicates of each surface type. Cells were fixed with 4% formaldehyde, washed twice with PBS, dehydrated using a graded ethanol series (50%, 70%, 80%, 90%, 96%, and 100%), and air-dried overnight. To visualize the cells on the scaffolds, the discs were sputter-coated with gold, and examined using an accelerating voltage of 15 kV. Images were captured at randomly selected regions at 5000x magnification. An XFlash 6-30 Energy Dispersive Spectroscopy (EDS) system (Bruker, Billerica, Massachusetts, United States) was employed to detect carbon and confirm cells in contrast to scaffold material.

Metabolic activity of osteoblasts

The cell metabolic activity of osteoblasts was assessed using AlamarBlue® Cell Viability Reagent (Invitrogen, Rockford, IL, USA) at day 4 and 29. Cells were incubated with AlamarBlue® reagent in culture medium (1:10, v/v) in a humidified incubator with 5% CO_2 in air at 37°C for 4 h. After incubation, 200 μl of supernatant was transferred into a 96-well plate (Company, City, Country). The absorbance was measured at 530 nm using a Synergy HT® spectrophotometer (BioTek instruments, Winooski, VT, USA). Data were obtained from three donors (n = 3), with experiments in duplicate.

Alkaline phosphatase activity

Alkaline phosphatase (ALP) activity was determined to assess the osteoblastic phenotype of the cells cultured on different surface on day 4, 7, 11, 15, 19, 22, and 25. Cells were lysed with 1.5 mL milli-Q water, and stored at −20°C until use. 4-Nitrophenyl phosphate disodium salt (Merck, City, Country) at pH 10.3 was used as a substrate for ALP, according to Lowry's method.[14] The absorbance was

measured at 405 nm using a Synergy HT® spectrophotometer (BioTek Instruments, Santa Clara, United states). ALP activity was expressed as nmol/µg cellular protein. BCA Protein Assay Reagent Kit (Pierce™) was utilized to measure the amount of protein. The absorbance was read at 540 nm with a Syngergy HT® spectrophotometer. Data were obtained from three donors (n = 3), with experiments in duplicate.

Qualification of extracellular matrix mineralization

Mineral deposition in the extracellular matrix was visualized using tetracycline hydrochloride (TC)-staining.[15] A TC (Sigma-Aldrich) solution [10 mg/mL] was prepared in PBS and administered to the cells at a final concentration of 20 µg/mL in the culture medium, followed by overnight incubation on days 7, 14, and 21. After 29 days, all discs were fixed in 4% formaldehyde for 15 minutes and washed with PBS. Newly deposited mineralization was visualized using a Nikon AXR laser confocal microscope (Nikon Europe, Amstelveen, Netherlands), using a 405 nm laser for excitation and recording emission between 420 and 470 nm, as described before.[15] Overviews were captured using a Plan Apo λD 4x objective, and 3 random locations per disc were recorded using a Plan Apo λD 10x objective, with consistent acquisition settings. Linear adjustments to brightness and contrast were made using ImageJ,[16] and data were presented qualitatively with representative images.

CD14+ monocyte isolation

The number and differentiation of osteoclasts in response to osteoblast-CM were evaluated after culturing isolated CD14+ monocytes for 7, 14, and 21 days. CD14+ monocytes were obtained from a buffy coat containing peripheral blood mononuclear cells from one patient (Sanquin, Amsterdam, The Netherlands). The isolation of CD14+ monocytes was performed using Lymphoprep density gradient centrifugation (Alere Technologies, Oslo, Norway), a manual magnetic-assisted cell sorter (MACS), and iron-conjugated CD14 antibodies (Miltenyi Biotec, Bergisch Gladbach, Germany) to isolate CD14+ monocytes, as previously described.[17] The isolated CD14+ monocytes (10×10^3 cells/well) were seeded into 41 wells per plate across three 96-well plates (Greiner Bio-One), totaling 123 wells. For each plate, 5 wells were designated as the control group, and 9 wells (3 per osteoblast donor) were assigned to each surface modification from the osteoblast experiments. During the first 3 days, each well received 0.12 mL of culture medium (α-MEM, 10% FBS, 1% PSF) supplemented with 25 ng/mL Macrophage colony-stimulating factor (M-CSF; R&D Systems). After this period, the medium was replaced with group-specific formulations for the remaining 21 days. The control group received medium containing 10 ng/mL M-CSF and 5 ng/mL receptor activator of nuclear factor kappa-B ligand (RANKL; R&D Systems). In contrast, the wells assigned to surface modifications received a 1:1 ratio of culture medium (with 20 ng/mL M-CSF and 10 ng/mL RANKL) and osteoblast-CM collected from the 3 osteoblast donors on day 29 of the experiment. Thus, between days 3 and 21, all wells received the same concentrations of M-CSF and RANKL. Media were replaced twice a week, and cells were incubated at 37°C and 5% CO2.

Osteoclast resorptive activity

The differentiation of the osteoclasts was quantified by measuring the extracellular secretion of Tartrate-resistant acid phosphatase (TRAP) during osteoclast culture. Supernatants were collected, and TRAP was measured using a colorimetric assay. The samples were incubated with p-nitrophenyl phosphate (pNPP) as a substrate in an acidic buffer at 37°C for 1 hour. After the reaction, the conversion of pNPP into p-nitrophenol was halted using sodium hydroxide. The resulting color change was measured at 405 nm using a Synergy HT® spectrophotometer, with a reference positive control for comparison. TRAP activity was quantified by comparing the absorbance to a standard curve of p-nitrophenol and expressed as nanomoles of p-nitrophenol produced per microgram of extracellular protein. Data were obtained from three independent experiments (n = 3) in duplicate.

Osteoclastogenesis and formation

The CM from each donor was applied in triplicate wells per group. After 7, 14, and 21 days, all cells from a single 96-well plate were fixed with 4% formaldehyde (Sigma-Aldrich) and stained with Tartrate Resistant Acid Phosphatase (TRACP), using a Leukocyte Acid Phosphatase staining kit (Sigma-Aldrich), as described previously.[18] Diamidino-2-phenylindole dihydrochloride (DAPI; Thermo Fisher Scientific) was used to counterstain cell nuclei. Osteoclasts were identified by positive TRACP staining, counted and categorized based on the number of nuclei per cell: 3-5 nuclei, and more than 5 nuclei. Bright field and fluorescent microscopy (Leica, Wetzlar, Germany) were used to capture microscopic images (10x magnification) from 5 consistent areas in each well: one from the center, two from the left and right edges, and two from the top and bottom along the vertical midline. Data were obtained from three donors (n = 3), with experiments in triplicate.

Statistical analysis

The distribution of data across all experiments and groups was evaluated using quantile-quantile (Q-Q) plots and the Shapiro-Wilk test. All experiments, except for the osteoclast

count experiment, exhibited highly skewed distributions. To approximate normality, a log-transformation was applied to the skewed data. This transformation enabled the calculation of the mean and the log-transformed 95% confidence intervals (CI), as previously recommended in the literature.[19] In case of normally distributed data, the mean and 95%CI were calculated. Non-overlapping CIs indicate a significant difference, whereas overlapping CIs indicate non-significance. The log-transformation and data visualization were performed using RStudio (version 4.0.3; RStudio, Boston, MA, USA). If no significant differences were found between the three VPS-HA modifications, their data were pooled into a single VPS-HA group for comparison against the trabecular surface. For the osteoclastogenesis and activation analyses, the number of osteoclasts and multinucleation were also compared to the control group to evaluate the baseline effects of osteoblast-CM on osteoclasts. Each experimental unit (n = 1) corresponds to an independent osteoblast donor. Within each experiment, replicates were conducted under identical conditions to ensure data consistency and reliability.

Results

Cell viability and seeding efficiency of osteoblasts

The mean percentage of viable osteoblasts prior to seeding was comparable across all surfaces: VPS350-HA (90.0%, CI 87.7–92.3), VPS400-HA (87.8%, CI 85.1–90.5), VPS1000-HA (91.0%, CI 88.0–93.9), and trabecular (88.1%, CI 84.2–92.1). Similarly, seeding efficiency was consistent between surfaces, with VPS350-HA at 87.3% (CI 81.1–93.4), VPS400-HA at 91.7% (CI 88.9–94.5), VPS1000-HA at 91.9% (CI 88.3–95.6), and trabecular at 92.0% (CI 87.3–96.6). On day 4, SEM imaging (Figure 1) confirmed osteoblast attachment on all scaffolds, regardless of surface type, at three random locations per scaffold.

Osteoblast metabolic activity and proliferation

The mean metabolic activity and CIs, measured by relative absorbance log, were similar at both day 4 and day 29 across the VPS350-HA, VPS400-HA, and VPS1000-HA surfaces (Table S-2), allowing the data from the three types to be pooled for comparison with the trabecular Ti6Al4V surface. The trabecular surface exhibited significantly higher metabolic activity, with a 1.5-fold increase over pooled VPS-HA values at day 4 and a 2.7-fold increase at day 29 (Figure 2, Table S-2).

Alkaline phosphatase activity and qualification of mineralization

Mean ALP activity (log nmol/µg protein) and CIs were similar across VPS350-HA, VPS400-HA, and VPS1000-HA surfaces at all measured timepoints (Table S-3), allowing the data to be pooled for comparison with the trabecular Ti6Al4V surface. The trabecular Ti6Al4V surface consistently exhibited significantly higher ALP activity throughout the experiment, with increases ranging from 6.5- to 15.2-fold compared to the pooled VPS-HA surfaces (Figure 3, Table S-3). By day 29, all scaffolds across surface types exhibited fluorescence under laser confocal microscopy at 10x magnification and overview captures, confirming mineral deposition (green), which indicates that osteoblasts maintained their phenotype throughout the experiment (Figure 1). The fluorescence intensity observed on the trabecular surface was lower compared to the VPS-HA surfaces, requiring adjustments to the contrast range (0-1500 to 150-200 lux) for enhancing visualization (Figure 1).

Extracellular secreted tartrate-resistant acid phosphatase by osteoclasts

Osteoclasts cultured without osteoblast-CM (control) exhibited no detectable TRAP activity (log nmol/µg protein) at day 15, which increased to 0.09 (95% CI: 0.06–0.13) at day 19 and 0.34 (95% CI: 0.25–0.42) at day 21 (Figure 4, Table S-4). For the VPS350-HA, VPS400-HA, and VPS1000-HA surfaces, secreted TRAP activity values were comparable at days 15 and 19. However, at day 21, VPS350-HA exhibited significantly lower secreted TRAP activity (3.2- to 3.5-fold) compared to VPS400-HA and VPS1000-HA (Table S-4). The trabecular Ti6Al4V surface scaffolds demonstrated mean secreted TRAP activity levels comparable to those of the pooled VPS-HA surfaces throughout the experiment (Figure 4, Table S-4).

Osteoclastogenesis and formation

The mean number of osteoclasts per mm^2 cultured without osteoblast-CM (control) was consistently higher in the 3–5 nuclei category compared to the >5 nuclei category at day 7, 14 and 21 (Figure 5, Table S-5). This trend was also observed in the number of osteoclasts with osteoblast-CM from any other surface modification. Osteoclast counts per mm^2 were comparable across the VPS350-HA, VPS400-HA, and VPS1000-HA surfaces at each time point, regardless of nuclei category (Table S-5), allowing the data to be pooled for comparison with the trabecular Ti6Al4V surface (Figure 5). The pooled VPS-HA surfaces exhibited similar mean osteoclast counts per mm^2 across both nuclei categories compared to the trabecular surface at day 7 (Figure 5, Table S-5). However, at day 14, the VPS-HA surfaces showed significantly higher mean osteoclast counts, with 2.1-fold and 2.6-fold increases for the 3–5 and >5 nuclei categories, respectively. By day 21, these differences further increased to 3.1-fold and 3.4-fold,

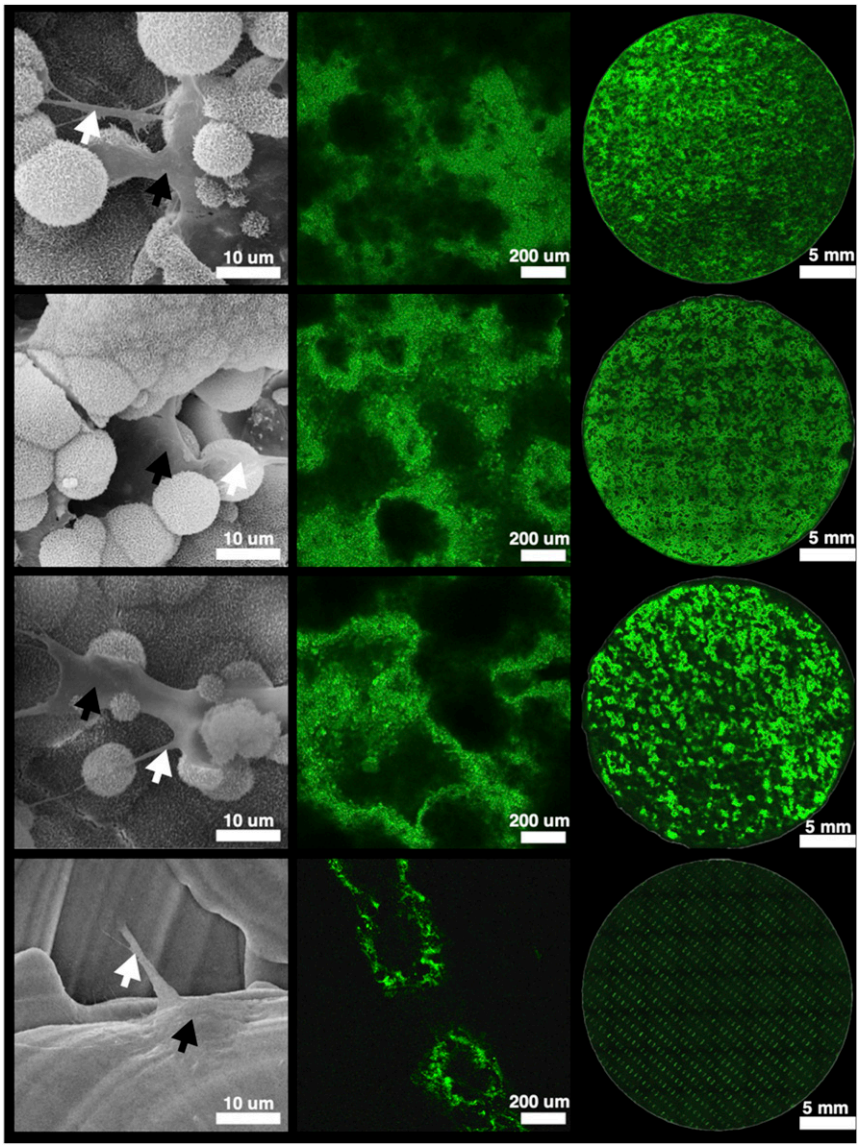

Figure 1. Scanning Electron Micrographs (SEM), laser confocal microscope single-view images at 10x magnification, and overview captures of mineralization patterns of osteoblast cultures on scaffold surfaces. Scaffold rows (top to bottom): (1) VPS350-HA, (2) VPS400-HA, (3) VPS1000-HA, and (4) trabecular surface. Left column: SEM images showing scaffold surfaces on day 4. Black arrows indicate osteoblasts, and white arrows highlight filopodia interacting with the substrate. Energy Dispersive Spectroscopy confirmed that the observed material on the surfaces was of cellular origin. SEM settings: 20.00 kV accelerating voltage, ×5000 magnification. Middle column: Laser confocal microscope images showing single-view fluorescent staining of mineral deposition by osteoblasts on day 29 using tetracycline hydrochloride. Tetracycline fluorescence was detected at 405 nm excitation, with emission recorded between 420 and 470 nm. Right column: Overview captures illustrating mineralization patterns across the entire scaffold surface on day 29. Fluorescent staining was achieved using tetracycline hydrochloride, which binds to newly deposited minerals, providing a precise visualization of active bone formation. Contrast ranges were set at 0–1500 lux for VPS-HA surfaces and 150–200 lux for trabecular surfaces to enhance visualization.

respectively, compared to the trabecular surface (Figure 5, Table S-5).

Discussion

For successful rigid fixation in uncemented TKR, it is critical that bone formation by osteoblasts outweighs bone resorption by osteoclasts, ensuring a net gain in bone mass while minimizing resorptive activity. To model this, we used three human osteoblast donors with characteristics similar to typical TKR patients—older adults, predominantly women. These characteristics are particularly relevant, as aging significantly impacts osteosynthesis at the bone–implant interface, potentially influencing the success of

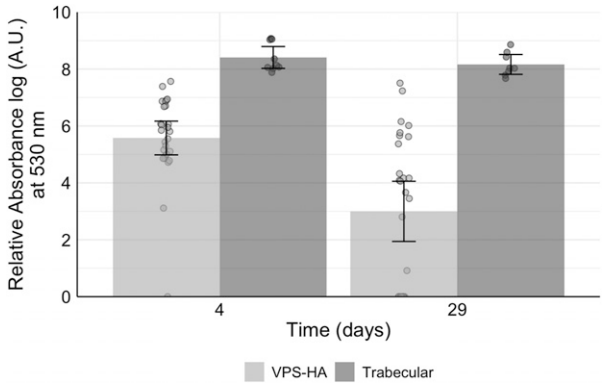

Figure 2. Metabolic activity and proliferation of human osteoblasts cultured on pooled VPS-HA (VPS350-HA, VPS400-HA, VPS1000-HA) and trabecular surfaces at days 4 and 29. Data from the three VPS-HA surfaces were pooled due to their comparable metabolic activity, with separate data presented in the supplemental file (Table S-2). The graph shows log-transformed data to account for distribution differences. Bars represent the mean absorbance (at 530 nm), while error bars indicate the 95% confidence intervals. Data points within the figure represent individual data values. Results were derived from three independent experiments (n = 3), each performed in duplicate. The trabecular surface showed significantly higher absorbance at both day 4 and day 29 compared to the pooled VPS-HA surfaces.

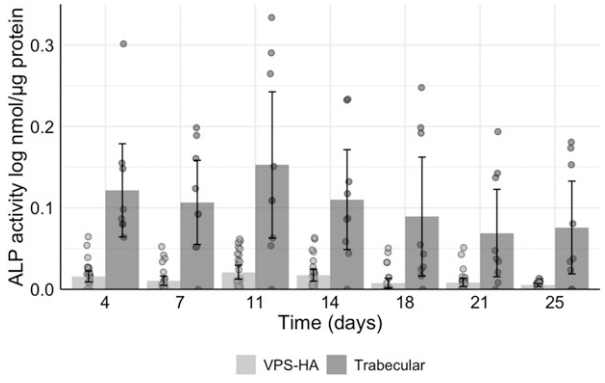

Figure 3. Alkaline phosphatase activity (ALP) of human osteoblasts cultured on pooled VPS-HA (VPS350-HA, VPS400-HA, VPS1000-HA) and trabecular surfaces. Data from the three VPS-HA surfaces were pooled due to their comparable ALP activity, with separate data provided in the supplemental file (Table S3). Bars represent the mean log-transformed ALP activity to account for distribution differences, with error bars showing the 95% confidence intervals. Individual data points within the figure represent measurements from three independent experiments (n = 3), each performed in duplicate. The trabecular surface demonstrated significantly higher ALP activity compared to the pooled VPS-HA surfaces, indicating enhanced osteoblast differentiation.

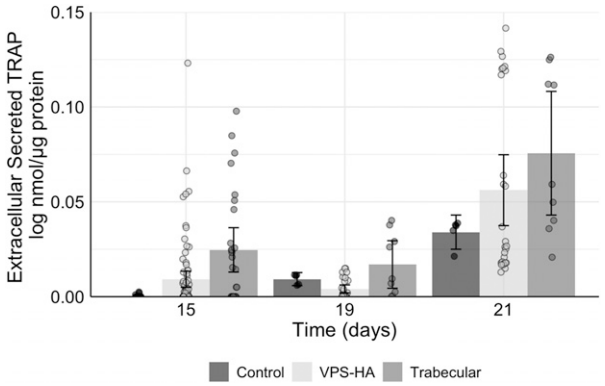

Figure 4. Extracellular secreted tartrate-resistant acid phosphatase (TRAP) activity of human osteoclasts cultured without conditioned medium (CM) (Control) and with CM of osteoblasts cultured on pooled VPS-HA (VPS350-HA, VPS400-HA, VPS1000-HA) and trabecular surfaces. Data from the three VPS-HA surfaces were pooled due to their comparable TRAP activity, with separate data provided in the supplemental file (Table S-4). Bars represent the mean log-transformed TRAP activity to account for distribution differences, with error bars showing the 95% confidence intervals. Individual data points within the figure represent measurements from three independent experiments (n = 3), each performed in duplicate. Results indicate no significant differences in TRAP activity between groups. Osteoclasts cultured without osteoblast-CM (control) exhibited no detectable TRAP activity at day 15, but it increased over time, reaching the highest levels at day 21. The trabecular surface demonstrated comparable TRAP activity to the pooled VPS-HA surfaces throughout the experiment.

uncemented TKR fixation.[20] The aim of this study was to evaluate human osteoblast differentiation and osteoclast activation mediated by CM from osteoblasts cultured on VPS-HA and trabecular surfaces.

Initially, we compared three VPS-HA surface types with varying porosity (20%–40%, 30%–70%, 30%–70%) and HA-coating thickness (60, 90, and 80 µm, respectively), tailored to meet the depths of pockets on specific implant locations. Despite these differences, no significant variations were observed in osteoblast viability, seeding efficiency, metabolic activity, alkaline phosphatase activity, osteoclast-secreted TRAP, or osteoclast formation among the VPS-HA surfaces. This suggests that VPS-HA surface variations in porosity and HA-coating thickness minimally affect osteoblast and osteoclast behavior in these conditions, allowing data from the three surfaces to be pooled for comparison with the trabecular surface.

The comparability between the VPS-HA surfaces may result from the pore-filling effect of HA-coating application. Borsari et al. studied MG-63 osteosarcoma proliferation and differentiation on VPS-Ti scaffolds with varying porosities, both with and without HA coatings.[4] They found that HA coatings reduced porosity by 4- to 6-fold and concluded that HA coatings synergistically enhance cellular responses only

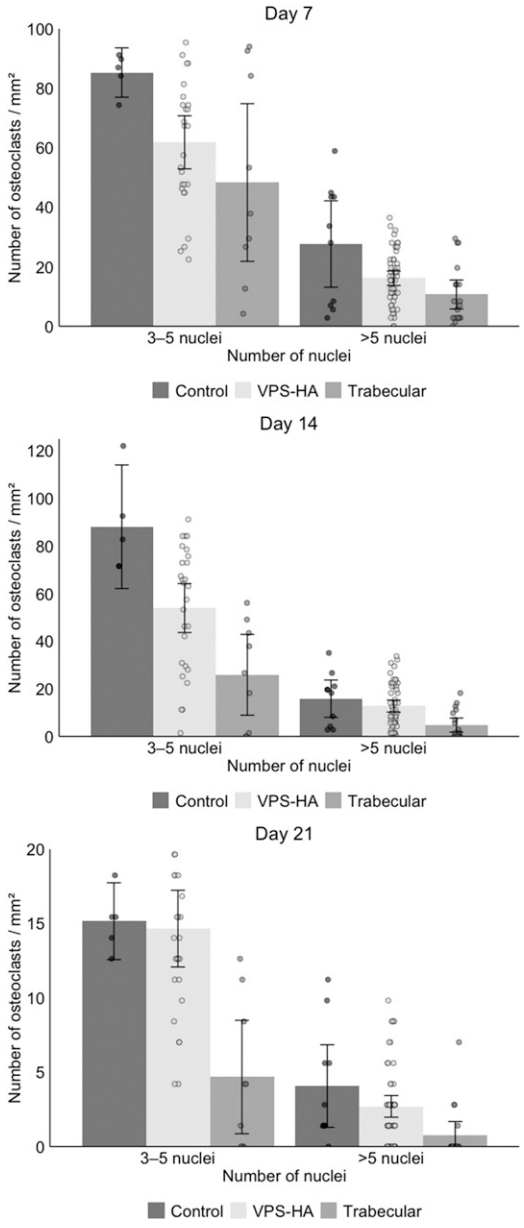

Figure 5. Osteoclastogenesis and formation of Tartrate-Resistant Acid Phosphatase (TRAP)-stained multinucleated human osteoclasts at Days 7, 14, and 21, cultured on polystyrene without conditioned medium (CM) (Control) and with CM from osteoblasts cultured on pooled VPS-HA (VPS350-HA, VPS400-HA, VPS1000-HA) and trabecular surfaces. Diamidino-2-phenylindole dihydrochloride (DAPI) was used to counterstain cell nuclei. Data from the three VPS-HA surfaces were pooled due to their comparable osteoclastogenic formation, with separate data provided in the supplemental file (Table S-5). Bars represent the mean number of osteoclasts per mm^2, with error bars showing the 95% confidence intervals. Individual data points within the figure represent measurements from three independent experiments (n = 3), each performed in triplicate. Results indicate that at Days 14 and 21, the trabecular surface exhibited a significantly lower number of osteoclasts compared to the pooled VPS-HA surfaces.

when applied to surfaces with lower roughness.[4] Further, all scaffolds, regardless of porosity and coating, exhibited similar levels of differentiation, indicated by ALP activity and C-terminal type I procollagen (PICP).[4] Similarly, in our study, the HA coatings may have masked surface variations, resulting in similar osteoblast and osteoclast responses across the VPS-HA surfaces. Nevertheless, HA-coatings are widely recognized for improving implant stability, as evidenced by reduced migration in RSA studies, and enhancing durability in uncemented TKR.[21,22] The HA-coating thicknesses in the current study (60–90 µm) align with the optimal range (70–90 µm) reported for osseointegration.[23] In orthopedic surgery, however, thinner rather than thicker HA coatings are generally preferred due to concerns about coating fatigue, instability, and wear, which may compromise long-term implant performance.[21,24]

Compared to VPS-HA surfaces, the trabecular surface exhibited significantly higher osteoblast metabolic activity and differentiation (ALP activity) throughout the experiment. Research shows that a minimum pore size of 300 µm is required to enhance osseointegration effectively, with osteoblasts growth occurring best in pore sizes of 600 µm diameter, rather than other diameters in the 300-1000 µm range.[5,25] In our study, the trabecular surface features pores ranging from 450 to 900 µm, with the sizes varying throughout the interconnected pore network to facilitate cell attachment, migration, vascularization, and nutrient exchange, while also reducing the risk of growth arrest, making it particularly advantageous for early fixation and long-term stability.[25,26] This structural advantage may also have contributed to the observed reduction in osteoclast multinucleation and formation, potentially through osteoblast-CM containing factors that suppressed resorption and promoted bone formation.

These findings align with a large RSA meta-analysis of 4706 TKRs, which demonstrated superior early stability of trabecular and HA-coated implants compared to uncoated and porous-surfaced implants.[22] A long-term Dutch registry study reported a 10-year revision rate for aseptic loosening of 0.2% (CI 0.0–0.4) across 1140 HA-coated TKR systems, encompassing multiple implant designs.[11] Trabecular implants were not included due to insufficient sample size.[11] The uncemented Global Medacta Knee TKR with 'MectaGrip'[13] (VPS-HA) surface technology has been used 1934 times in Australia, as documented in the 2024 annual AOANJRR registry report.[27] Its 10-year revision rate for any reason is 5.8% (CI 4.4–7.6), exceeding the ODEP 10-year benchmark of 5.0%.[27,28] This rate includes revisions for reasons beyond aseptic loosening. Unfortunately, the specific trabecular "3D-metal" technique has not yet been implemented for uncemented TKR by Medacta, and therefore no revision rates specific to this implant are currently available. However, other uncemented TKR implants featuring a similar trabecular surface design, such as

the NexGen Trabecular Metal, have shown promising results. According to a Finnish registry study, the NexGen Trabecular Metal demonstrated a 7-year revision rate for any reason of 3.0% (CI 2.0–4.0) and 0.0% (CI 0.0–1.0) for aseptic loosening.[29] Regarding the Global Medacta Knee with 'MectaGrip'[13] (VPS-HA) surface technology, further clinical research into the failure mechanisms is required, ideally through RSA and survival studies. Such studies should ideally precede widespread clinical use to minimize the risk of unnecessary revisions.

In this study, all four surface groups demonstrated mineralization at day 29, shown by TC-staining; however, the fluorescence intensity was lower on the trabecular surface compared to the VPS-HA surfaces (Figure 1). This difference could be due to actual variations in mineralization, the inability of the laser confocal microscope to detect fluorescence from deeper pores in the trabecular structure, or the possibility of TC binding to the HA coating rather than newly formed minerals. Despite this, slower mineralization is unlikely to explain the findings, as previous RSA studies have shown earlier stabilization of trabecular-surfaced implants compared to other surface modifications.[22] In an attempt to ensure accurate visualization of mineralization, we used a TC-staining, as a previous study reported it to directly bind to newly deposited minerals, unlike other methods such as alizarin-red staining, which can stain pre-existing HA coatings or other matrix components.[15,30] This approach enhances confidence that the observed fluorescence reflects active bone formation across the different surface types.[15]

Osteoclast differentiation and activity, as indicated by secreted TRAP levels in the supernatant, did not significantly differ between VPS-HA surfaces, nor between the pooled VPS-HA group and the trabecular surface in this study. TRAP secretion is a well-established marker of resorptive behavior in osteoclasts. However, Kirstein et al. demonstrated that a mineralized substrate is essential for the full activation and resorptive response of osteoclasts.[31] In our study, osteoclasts were cultured on polystyrene, which lacks a mineralized substrate and likely inhibited their resorptive response. This limitation is underscored by the observation that, despite similar secreted TRAP levels across surfaces, the osteoclast count was significantly lower on the trabecular surface compared to the pooled VPS-HA surfaces. This difference could be due to non-measured osteoblast-derived factors present in the osteoblast-CM, as osteoblasts are known to secrete factors that modulate osteoclast behavior beyond the effects of RANKL and M-CSF alone.[32]

This study has several limitations. First, the base alloys differed between groups (CoCrMo vs. Ti6Al4V). While cobalt ions are known to negatively impact osteoblast behavior,[33] their release is unlikely within such a short study duration. Moreover, CoCrMo alloys are widely used clinically, accounting for 47%–96% of components in the Dutch Arthroplasty Registry, which justifies the clinically relevant comparison.[34] Second, the number of seeded osteoblasts varied due to the larger surface area of the trabecular surface, which may have influenced the results. However, in clinical applications, trabecular implants also provide greater surface area and bone contact, aligning with the comparisons made in this study. Third, meaningful statistical quantification of osteoblast attachment via SEM imaging or matrix deposition through laser confocal microscopy was not feasible due to the significant geographic differences among the surface modifications. However, the primary focus was to confirm the presence of mineralization across all surfaces, ensuring that the osteoblast-CM contained osteoblast-derived factors necessary to provide a consistent baseline for the subsequent osteoclast experiments.

Conclusion

This study demonstrates that variations in VPS Ti surface porosity and HA-coating thickness have minimal impact on osteoblast differentiation and osteoclast activation. Conversely, the findings revealed that the trabecular Ti6Al4V surface provides a more favorable in vitro environment than the VPS-HA surfaces, enhancing osteoblast differentiation and reducing osteoclast multinucleation, indicating a shift toward bone formation over resorption. These findings highlight the potential advantages of trabecular surfaces in promoting early implant stability and reducing long-term aseptic loosening risks in uncemented TKRs. Nonetheless, further research is required to confirm these in vitro observations and assess their clinical implications in uncemented TKR applications.

Acknowledgments

This investigator-initiated study received no specific funding or grants from public, commercial, or not-for-profit sectors. All authors declare that they have no professional or financial affiliations that could be perceived as having biased the presentation of this study. This investigator-initiated research was conducted independently, without any influence from commercial entities or financial interests that could affect the study outcomes. We thank Medacta International for providing the scaffolds with specified surface structures for this study. Our gratitude also goes to Arie Werner for his technical support with the scanning electron microscope (SEM) and to the staff of the Microscopy & Cytometry Core Facility (MCCF) at Amsterdam UMC for their assistance with laser confocal microscopy.

Author contributions

Raymond Puijk: Conceptualization; data acquisition; analysis; interpretation; methodology; writing-original draft; writing-review

and editing. Behrouz Zandieh-Doulabi: Conceptualization; data acquisition; interpretation; methodology; writing-review and editing. Wendy J.A.M. Runderkamp: Data acquisition; methodology; writing-review and editing. Bart G. Pijls: Conceptualization; data interpretation; writing-review and editing. Jenneke Klein-Nulend: Conceptualization; writing-review and editing. Peter A. Nolte: Conceptualization; data interpretation; writing-review and editing. All authors have read and approved the final submitted manuscript.

Declaration of conflicting interests

The author(s) declared no potential conflicts of interest with respect to the research, authorship, and/or publication of this article.

Funding

The author(s) received no financial support for the research, authorship, and/or publication of this article.

Ethical statement

Ethical approval

Ethical approval and informed consent were not required for this study because it utilized commercially purchased cells from patients

Informed consent

Who had provided informed consent at the time of donation.

ORCID iD

Raymond Puijk https://orcid.org/0000-0002-0953-0070

Data Availability Statement

The data from this study is available upon request from the author.

Supplemental Material

Supplemental Material for this article is available online.

References

1. Klug A, Gramlich Y, Rudert M, et al. The projected volume of primary and revision total knee arthroplasty will place an immense burden on future health care systems over the next 30 years. *Knee Surg Sports Traumatol Arthrosc* 2021; 29: 3287–3298.
2. Hussain M, Askari Rizvi SH, Abbas N, et al. Recent developments in coatings for orthopedic metallic implants. *Coatings (Oakv)* 2021; 11: 791.
3. Osman MA, Alamoush RA, Kushnerev E, et al. In-vitro phenotypic response of human osteoblasts to different degrees of titanium surface roughness. *Dent J* 2022; 10: 140.
4. Borsari V, Giavaresi G, Fini M, et al. Physical characterization of different-roughness titanium surfaces, with and without hydroxyapatite coating, and their effect on human osteoblast-like cells. *J Biomed Mater Res B Appl Biomater* 2005; 75: 359–368.
5. Frosch KH, Barvencik F, Viereck V, et al. Growth behavior, matrix production, and gene expression of human osteoblasts in defined cylindrical titanium channels. *J Biomed Mater Res* 2004; 68: 325–334.
6. Puijk R, Singh J, Puijk RH, et al. Evaluation and refinement of thresholds for early migration of total knee replacements as an estimator of late aseptic loosening: an updated systematic review of RSA and survival studies. *Acta Orthop* 2025; 96: 1–10.
7. Ryd L, Albrektsson BE, Carlsson L, et al. Roentgen stereophotogrammetric analysis as a predictor of mechanical loosening of knee prostheses. *J Bone Joint Surg Br* 1995; 77: 377–383.
8. Tang Z, Xie Y, Yang F, et al. Porous tantalum coatings prepared by vacuum plasma spraying enhance BMSCs osteogenic differentiation and bone regeneration in vitro and in vivo. *PLoS One* 2013; 8: e66263.
9. *Knee joint patellofemorotibial and femorotibial metal/polymer porous-coated uncemented prostheses - class II special controls guidance document for industry and FDA*: FDA. https://www.fda.gov/medical-devices/guidance-documents-medical-devices-and-radiation-emitting-products/knee-joint-patellofemorotibial-and-femorotibial-metalpolymer-porous-coated-uncemented-prostheses
10. Polizzotti G, Lamberti A, Mancino F, et al. New horizons of cementless total knee arthroplasty. *J Clin Med* 2024; 13: 233.
11. Puijk R, Rassir R, Sierevelt IN, et al. Association between surface modifications for biologic fixation and aseptic loosening of uncemented Total Knee Replacements. *J Arthroplast* 2023; 12: 2605–2611.
12. Nagendrababu V, Murray PE, Ordinola-Zapata R, et al. PRILE 2021 guidelines for reporting laboratory studies in Endodontology: a consensus-based development. *Int Endod J* 2021; 54: 1482–1490.
13. Medacta international - 3D metal and MectaGrip. https://www.medacta.com/EN/global-advanced-materials
14. McComb RB, Bowers GN and Posen S. Measurement of alkaline phosphatase activity. *Alkaline Phosphatase* 1979; 29: 289–372.
15. Macri-Pellizzeri L, De Melo N, Ahmed I, et al. Live quantitative monitoring of mineral deposition in stem cells using tetracycline hydrochloride. *Tissue Eng Part C* 2018; 24: 171–178.
16. Schindelin J, Arganda-Carreras I, Frise E, et al. Fiji: an open-source platform for biological-image analysis. *Nat Methods* 2012; 9: 676–682.
17. ten Harkel B, Schoenmaker T, Picavet DI, et al. The foreign body giant cell cannot resorb bone, but dissolves hydroxyapatite like osteoclasts. *PLoS One* 2015; 10: e0139564.
18. de Vries TJ, Schoenmaker T, Micha D, et al. Periodontal ligament fibroblasts as a cell model to study osteogenesis and osteoclastogenesis in fibrodysplasia ossificans progressiva. *Bone* 2018; 109: 168–177.

19. Amrhein V, Greenland S and McShane B. Scientists rise up against statistical significance. *Nature* 2019; 567: 305–307.
20. Pius AK, Toya M, Gao Q, et al. Effects of aging on osteosynthesis at bone-implant interfaces. *Biomolecules*; 14: 52.
21. Voigt JD and Mosier M. Hydroxyapatite (HA) coating appears to be of benefit for implant durability of tibial components in primary total knee arthroplasty. *Acta Orthop* 2011; 82: 448–459.
22. Puijk R, Puijk RH, Laende EK, et al. 6-month migration sufficient for evaluation of total knee replacements: a systematic review and meta-analysis. *Acta Orthop* 2023; 94: 577–587.
23. Nuswantoro NF, Gunawarman MM, Manjas M, et al. Effect of hydroxyapatite coating thickness on inflammation and osseointegration of Ti–29Nb–13Ta-4.6Zr (TNTZ) implants. *J Mater Res Technol* 2024; 30: 6210–6217.
24. Pijls B, Valstar ER, Kaptein B, et al. The beneficial effect of hydroxyapatite lasts. *Acta Orthop* 2012; 83: 135–141.
25. Regis M, Marin E, Fedrizzi L, et al. Additive manufacturing of Trabecular Titanium orthopedic implants. *MRS Bull* 2015; 40: 137–144.
26. Perez RA and Mestres G. Role of pore size and morphology in musculo-skeletal tissue regeneration. *Mater Sci Eng C* 2016; 61: 922–939.
27. Australian Orthopaedic Association National Joint Replacement Registry (AOANJRR). Hip, knee & shoulder arthroplasty: annual report 2024. https://aoanjrr.sahmri.com/annual-reports-2024
28. Orthopaedic data evaluation panel (ODEP) rating system. https://www.odep.org.uk/about/rating-system/
29. Niemeläinen M, Skyttä ET, Remes V, et al. Total knee arthroplasty with an uncemented trabecular metal tibial component: a registry-based analysis. *J Arthroplast* 2014; 29: 57–60.
30. Virtanen P and Isotupa K. Staining properties of alizarin red S for growing bone in vitro. *Acta Anat* 1980; 108: 202–207.
31. Kirstein B, Chambers TJ and Fuller K. Secretion of tartrate-resistant acid phosphatase by osteoclasts correlates with resorptive behavior. *J Cell Biochem* 2006; 98: 1085–1094.
32. Amarasekara DS, Yun H, Kim S, et al. Regulation of osteoclast differentiation by cytokine networks. *Immune Netw* 2018; 18: e8.
33. Anissian L, Stark A, Dahlstrand H, et al. Cobalt ions influence proliferation and function of human osteoblast-like cells. *Acta Orthop Scand* 2002; 73: 369–374.
34. The Dutch Arthroplasty Registry (LROI). Annual report 2022. https://www.lroi-report.nl